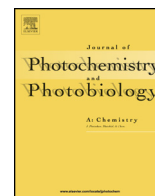




Contents lists available at ScienceDirect

Journal of Photochemistry and Photobiology A: Chemistry

journal homepage: www.elsevier.com/locate/jphotochem

2,5-bis[2-(2-phenyl-1,3-oxazol-5-yl)phenyl]-1,3,4-oxadiazole – new sterically hindered high Stokes shift fluorophore sensitive to media viscosity

Rodion Yu Iliashenko^a, Oleg O. Borodin^a, Michał Wera^b, Andrey O. Doroshenko^{a,*}^a Department of Chemistry, Kharkov V. N. Karazin National University, 4 Svobody Sqr., Kharkov 61022, Ukraine^b Faculty of Chemistry, University of Gdańsk, Wita Stwosza 63, Gdańsk 80-952, Poland

ARTICLE INFO

Article history:

Received 3 September 2014

Received in revised form 21 October 2014

Accepted 26 October 2014

Available online 31 October 2014

Keywords:

Oxazole

1,3,4-Oxadiazole

Steric hindrance

X-ray structural analysis

TDDFT

ESSA

Excited state structural relaxation

Abnormally high fluorescence Stokes shift

Time-resolved fluorescence

Viscosity sensing

ABSTRACT

New sterically hindered high Stokes shift polyheteroaromatic fluorophore (2,5-bis[2-(2-phenyl-1,3-oxazol-5-yl)phenyl]-1,3,4-oxadiazole, (**1**) belonging to the *ortho*-POPOP family was synthesized and its molecular structure was confirmed by X-ray and NMR data. Like any other *ortho*-POPOPs, the title molecule is substantially non-planar in the ground state owing to repulsion of its oxazole/oxadiazole cycles introduced in *ortho*-positions of the inner-chain benzene rings. Thus the intramolecular π -conjugation in **1** molecule is weakened in respect to its planar *para*-substituted analogs. Intermolecular π - π contacts in the crystalline lattice result in asymmetrization of the oxadiazole-phenyl-oxazole subunits of **1**, which reflects itself in significantly different angles between the planes of azole and their neighboring benzene rings. Quantum-chemical modeling of **1** revealed for this molecule the ground state symmetrization in fluid media with alignment of the inter-ring angles. The significant excited state planarization of the title molecule, which was predicted by our TD-DFT calculations as well, results in partial restoration of the disturbed ground state conjugation, in decrease of the structurally relaxed excited state energy and finally – in theoretically predicted and experimentally observed abnormally high fluorescence Stokes shifts. The excited state conformational changing of **1** requires high amplitude intramolecular motions, which should be affected by the local media viscosity. This was confirmed in our time-resolved fluorescence experiments, which demonstrate decrease of the excited state structural relaxation rate in alcohols of different viscosity: 2-propanol, ethylene glycol and glycerol. Special experiments in toluene–polystyrene system allow us to recommend the investigated compound as potential fluorescent viscosity sensor.

© 2014 Elsevier B.V. All rights reserved.

1. Introduction

The main advantage of the high Stokes shift (HSS) organic fluorophores over all the other ones is the minimization of the emitted light losses caused by reabsorption [1,2]. Thus, one can apply such compounds at much higher concentrations, this enlarges the field of their practical application. High fluorescence Stokes shift is critical, for example, for scintillator devices of large dimensions [3], solid state fluorophores including those applied in OLEDs [4,5], fluorescent sensing compounds [6], several biophysical [7] and analytical [8] applications, etc. Most of the known photophysical and photochemical mechanisms leading to the fluorescence Stokes shift increase [9] are accompanied by

efficient radiationless degradation: formation of excimers [10] and exciplexes [11], excited state conformational changes: planarization of biphenyls/oligophenyls [12,13] and intermolecular twisting of dialkylamino-compounds [14], excited state proton transfer [15,16], etc.

Excited state structural relaxation, leading to formation of more planar molecular structure from the initial less planar one, could be considered as the most prominent mechanism of the Stokes shift enlargement. It seems to guarantee lower radiationless deactivation despite of the common concept, that non-planarity does not favor high fluorescence quantum yields owing to more rapid intersystem crossing [17]. Being a concurrent photophysical process to radiationless decay, excited state planarization plays a role of a factor increasing the total fluorescence efficiency: the faster is flattening, the higher is the quantum yield [18].

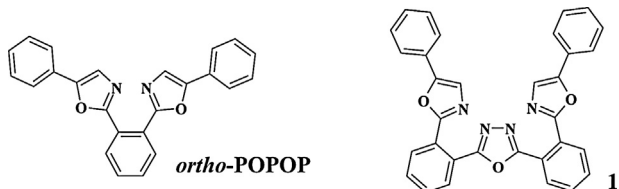
Several fluorescent systems with the excited state planarization are known, let us focus attention on compounds with bulky aromatic [19] or heteroaromatic [20] moieties in 1,2-positions of

* Corresponding author. Tel.: +380 57 707 5335; fax: +380 57 707 5130.

E-mail addresses: andrey.o.doroshenko@univer.kharkov.ua, andrey.o.doroshenko@gmail.com (A.O. Doroshenko).

the same benzene ring. Having (semi) helical molecular shape they undergo partial excited state planarization, which compresses helix to definite extent resulting in their experimentally observed abnormal fluorescence characteristics. Similar class of heteroaromatic compounds—*ortho*-analogs of the well-known organic fluorophore widely applicable in liquid an plastic scintillating devices, 1,2-bis(5-phenyl-1,3-oxazol-2-yl) benzene (POPOP) was studied in our research team during last decades: their synthesis [21,22] and X-ray structural analysis [23] was reported together with molecular modeling, spectral data [24,25] and photophysical experiments [26,27].

The present communication is devoted to the new representative of the *ortho*-POPOP family composed of the increased number of heteroaromatic units (7 except 5), 2,5-bis[2-(2-phenyl-1,3-oxazol-5-yl) phenyl]-1,3,4-oxadiazole, compound **1**:



Enlargement of the potential π -conjugation length is not the only question to resolve while synthesizing and studying of compound **1** spectral behavior and photophysics. The parent HSS-fluorophore of this series, *ortho*-POPOP, is practically a low-solvatochromic compound. Owing to the fact, that more electron-withdrawing oxadiazole cycle is included in **1** molecule, we expect intensification of the electron density redistribution during the electronic excitation and thus – appearance of higher sensitivity to solvent polarity.

Excited state planarization of the *ortho*-POPOP molecule requires high-amplitude intramolecular motions, this determines potential sensitivity of this compound also to media viscosity [26,28]. The title fluorophore **1** possesses two *ortho*-substituted benzene rings, thus its intramolecular rotors are characterized by higher moments of inertia, so we expect for it more pronounced sensitivity to viscosity in comparison to other *ortho*-POPOPs.

Traditionally, fluorescent monitoring of viscosity is based on compounds with intramolecular rotor moieties [29–31], however in most cases the proposed fluorophores (including commercially available ones [32]) are highly sensitive to media polarity as well. This makes fluorescent sensing of viscosity on their background less reliable, than it could be in the case of compounds with lower solvent polarity effects. Moreover, the above mentioned fluorescent viscosity probes realize the principles of intensometry and/or lifetime sensing: intensity of their fluorescence increases in more viscous surrounding without changing of color, simultaneous increase demonstrate fluorescence lifetimes. Compound **1** was expected to vary color of its fluorescence with viscosity, which makes it more convenient for various analytical applications.

2. Materials and methods

Compound **1** was synthesized by the following general scheme:



1.5 g (0.0057 mol) of 2-(2'-carboxyphenyl)-5-phenyl-1,3-oxazole [21,23] was boiled in 25 ml of thionyl chloride for 3 h until deflation of hydrogen chloride was finished, then SOCl_2 excess was removed in vacuo. Resulting acyl chloride was dissolved in 25 ml of pyridine and 0.37 g of hydrazine sulfate (0.003 mol) was added. The reaction mixture was boiled for 4 h, and then poured into 250 ml of cold distilled water. The deposited precipitate was filtered off, washed with water and dried on air. Final cyclization was made at its boiling in 25 ml of phosphorus oxychloride for 3 h, then cooled reaction mixture was poured in 200 g of ice. Final compound was purified by column chromatography (silica gel/benzene) and crystallized from heptane.

2,5-bis[2-(2-phenyl-1,3-oxazol-5-yl) phenyl]-1,3,4-oxadiazole, **1**, colorless needles, yield 0.94 g (63%), m.p. ~ 152 – 154 °C.

^1H NMR (500 MHz, DMSO-d_6): δ 8.17 (d, $J=7.8$ Hz, 2H), 7.82 (t, $J=7.7$ Hz, 2H), 7.79 (d, 2H, coupling constant is hardly detectable owing to overlap with the singlet peak at 7.78 ppm), 7.78 (s, 2H), 7.69 (t, $J=7.6$ Hz, 2H), 7.58 (d, $J=7.8$ Hz, 4H), 7.43 (t, $J=7.6$ Hz, 4H), 7.37 (t, $J=7.3$ Hz, 2H) ppm.

^{13}C NMR (126 MHz, DMSO-d_6) δ 164.57, 158.83, 151.81, 132.84, 131.48, 131.34, 130.02, 129.54, 129.35, 127.43, 126.95, 124.67, 124.44, 122.32 ppm.

Molecular structure of **1** was confirmed by X-ray structural analysis (Table 1).

The following computer software was used to treat the X-ray data: CrysAlis CCD and CrysAlis RED (Oxford Diffraction, 2008), SHELXS-2013 and SHELXL-2013 [34] for direct structure solving and refinement, ORTEP-3 [35] and PLATON [36] for structure visualization.

Atomic coordinates and crystallographic parameters have been deposited to the Cambridge Crystallographic Data Center (CCDC 1,020,369).

NMR spectra were measured on Bruker Avance III 500 spectrometer.

Electronic absorption and steady-state fluorescence spectra were measured on Hitachi U-3210 spectrophotometer and Hitachi 850 spectrofluorimeter in rectangular quartz cells with the dye solution layer thickness of 10 mm. Quinine sulfate in 0.5 M aqueous sulfuric acid was used as reference standard for estimating quantum yields [37].

Fluorescence decay and time-resolved fluorescence spectra were measured on home-composed sub-nanosecond kinetic spectrometer, consisting of a MDR-12 monochromator (LOMO, Russia), a TimeHarp 200 TCSPC device, a PLS 340-10 picosecond LED driven by a PDL 800-B device (PicoQuant GmbH, Germany) and a Hamamatsu H5783P PMT (Hamamatsu, Japan).

Normalized Reichardt solvent polarity index E_T^N [38] was applied for qualitative characterization of the polarity-dependent properties of the title compound.

3. Quantum-chemical modeling

Theoretical modeling was performed in DFT/TD-DFT schemes using the *b3lyp* hybrid potential [39] with the *cc-pvdz* basis [40]. Calculations of the molecular geometry and electron density redistribution upon electronic excitation of **1** were made with Gaussian-09 (release B.01 [41] – for the ground state molecular

Table 1
Crystallographic data for 2,5-bis[2-(2-phenyl-1,3-oxazol-5-yl) phenyl]-1,3,4-oxadiazole.

Crystal data	
Chemical formula	C ₃₂ H ₂₀ N ₄ O ₃
Molecular mass, <i>M_r</i>	508.53
Crystal system, space group	Orthorhombic, P2 ₁ 2 ₁ 2 ₁
Temperature (K)	295
Cell parameters, <i>a, b, c</i> (Å)	9.6294 (4), 13.4532 (7), 19.3356 (10)
Cell volume, <i>V</i> (Å ³)	2504.9 (2)
<i>Z</i>	4
Radiation type	Mo Kα, λ = 0.71073 Å
μ (mm ⁻¹)	0.09
Crystal size (mm)	0.65 × 0.1 × 0.1
Data collection	
Diffractometer	Oxford Diffraction Gemini R Ultra Ruby CCD
Absorption correction	Multi-scan (CrysAlis RED; Oxford Diffraction, 2008)
<i>T_{min}</i> , <i>T_{max}</i>	0.933, 0.988
Number of measured, independent and observed [<i>I</i> > 2σ(<i>I</i>)] reflections	9273, 4425, 2671
<i>R_{int}</i>	0.042
(Sin θ/λ) _{max} (Å ⁻¹)	0.596
Refinement	
<i>R</i> [<i>F</i> ² > 2σ(<i>F</i> ²)], <i>wR</i> (<i>F</i> ²), <i>S</i>	0.047, 0.081, 0.99
Number of reflections	4425
Number of parameters	352
H-atoms treatment	H atoms of C–H bonds were positioned geometrically, with C–H = 0.93 Å, and constrained to ride on their parent atoms with U _{iso} (H) = 1.2U _{eq} (C)
Δρ _{max} , Δρ _{min} (e Å ⁻³)	0.12, -0.13
Absolute structure	Flack x determined using 859 quotients [(<i>I</i> +) - (<i>I</i> -)]/[(<i>I</i> +) + (<i>I</i> -)] [33]
Absolute structure parameter	0.3 (10)

structure optimization) and NWChem (version 5.1 [42] equipped with special module for ESSA “excited state structural analysis” [43] – for the electronic spectra calculation) program packages.

4. Results and discussion

4.1. Molecular structure of the title compound in the crystalline state

X-ray molecular structure and atoms numbering scheme for compound **1** is shown in Fig. 1. Atom coordinates and important geometric parameters can be found in Supplementary section.

Similarly to the other *ortho*-POPOPs, molecule **1** in the crystalline lattice is substantially unplanar and asymmetric [21,23,27]. All its (hetero) aromatic cycles are planar indeed, but intercycle angles are substantially different. The central oxadiazole cycle (N2,N3,O2,C16,C17) makes with two neighboring phenyls the inter-plane angles of 62.0° (C10–C15) and 45.0° (C18–C23). Analogously, the angles between the inner phenylenes and the oxazole cycles planes are different as well: 15.5 and 28.5° correspondently. The less pronounced difference exists between the planes of the oxazole cycles and terminal benzene rings: 3.7 and 1.7°, thus the latter could be assumed as practically coplanar. Shortened intramolecular contacts (Fig. 1) between the *ortho*-hydrogen atoms of the terminal benzene rings and the oxazole cycles oxygen atoms (~2.50 Å) as well as between the inner phenylenes, *ortho*-hydrogens and the oxazoles nitrogen atoms (~2.58–2.60 Å) could not be the reason for such an asymmetry of the generally symmetric molecule of **1**.

In our early papers considering the crystalline structure of *ortho*-POPOPs we tried to find the energetic reasons for such an unusual behavior, however, arguments obtained there with semi-empirical quantum-chemical modeling [23,27] were really non-convincing: divergence in energy of different conformations of *ortho*-POPOP molecules was too low.

Thus, to clarify the asymmetrization of **1** in crystal lattice, intermolecular interactions should be considered. The corresponding scheme is shown in Fig. 2, while as packing of title molecule in

the crystalline state is presented in Fig. 1s of Supplementary section. Corresponding numerical data for weak unconventional intermolecular hydrogen bonds of C–H···O and C–H···π types and intermolecular π–π interactions are collected in Tables 2 and 3. Despite the low energy of each of them, acting together these weak interactions are forming unusually asymmetric molecular conformation of **1** in the crystalline state and systematic periodical structures with nearly parallel benzene rings of the neighboring molecules.

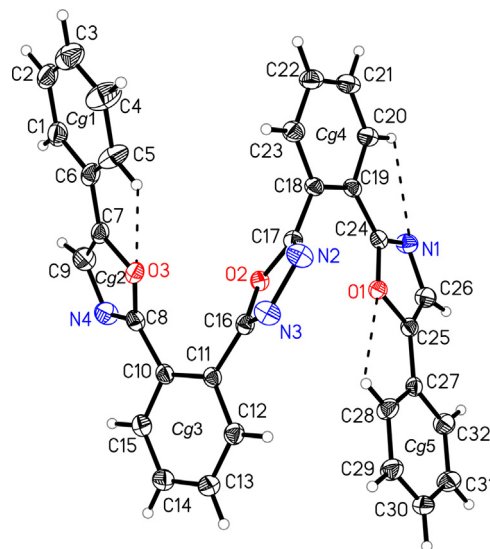


Fig. 1. The molecular structure of 2,5-bis[2-(2-phenyl-1,3-oxazol-5-yl) phenyl]-1,3,4-oxadiazole in the crystalline state and the atom-labeling scheme. Displacement ellipsoids are drawn at the 25% probability level and H atoms are shown as small spheres of arbitrary radius. The intramolecular C–H···O and C–H···N interactions are represented by dashed lines. Cg1, Cg2, Cg3, Cg4 and Cg5 denote the ring centroids.

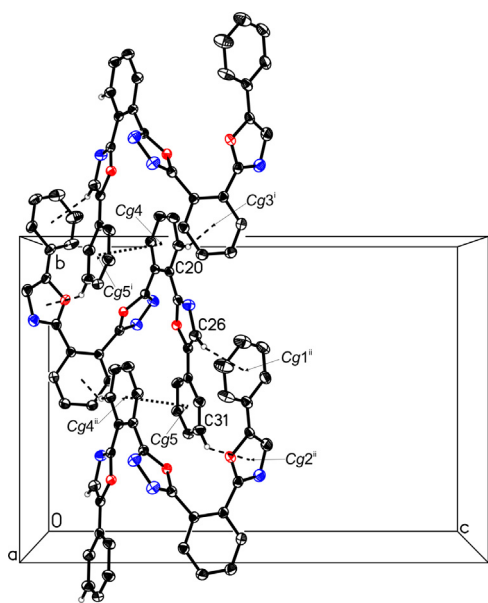


Fig. 2. Intermolecular interactions in the crystalline state of compound **1**. The C–H...O contacts are represented by dashed lines, the π – π contacts – by dotted lines. H atoms not involved in the interactions have been omitted. [Symmetry codes: (i) $-x+1, y+1/2, -z+1/2$; (ii) $-x+1, y-1/2, -z+1/2$].

4.2. Quantum-chemical modeling

Owing to the fact, that in the fluid state of dilute solution in organic solvent the above discussed intermolecular interactions are hardly possible, one should expect symmetrization of molecular conformation of the investigated compound. To have a general insight about the molecular structure of **1** in such conditions, a series of quantum-chemical calculations were made.

Ground state geometry optimization in *b3lyp/cc-pvdz* scheme started from the experimental X-ray geometry revealed its expected symmetry in non-restricted surrounding (this and the main alternative molecular conformations of **1** are shown in Table 6s, Supplementary section). The inter-cycle angles between the central oxadiazole cycle and attached to it benzene rings in the further discussed most probable molecular conformation of **1** were both equal to $\sim 38^\circ$. Each of the mentioned phenylene moieties forms an angle of $\sim 30^\circ$ with their “own” oxazole cycles. Correspondently, the angles between the planes of the oxazole cycles and the terminal benzene rings were found to be $\sim 5^\circ$.

Thus, the title molecule spatial dimensions and the π -conjugation extent both have to increase on going from the crystalline state to fluid media owing to the above discussed changes of the angles between the planes of its (hetero) aromatic cycles.

The experimental proton and carbon NMR spectra (see Section 2 and Supplementary section) confirm general symmetrization of **1** molecule on going from the crystalline state to fluid solutions (within the time scale of NMR spectroscopy): the total number of

Table 2

C–H... π intermolecular hydrogen bonds in the crystalline state of 2,5-bis[2-(2-phenyl-1,3-oxazol-5-yl) phenyl]-1,3,4-oxadiazole (\AA , $^\circ$).

D–H...A	D–H	H...A	D...A	D–H...A
C20–H20...Cg3 ⁱ	0.93	2.85	3.730 (4)	158
C26–H26...Cg1 ⁱⁱ	0.93	3.00	3.616 (6)	125
C31–H31...Cg2 ⁱⁱ	0.93	2.96	3.699 (5)	138

Cg1 denotes the centroid of the C1–C6 ring; Cg2 denotes the centroid of the O3, C7, N3, C9, C8 ring; Cg3 denotes the centroid of the C10–C15 ring. Symmetry codes: (i) $-x+1, y+1/2, -z+1/2$; (ii) $-x+1, y-1/2, -z+1/2$.

Table 3

Intermolecular π – π contacts in the crystalline state of 2,5-bis[2-(2-phenyl-1,3-oxazol-5-yl) phenyl]-1,3,4-oxadiazole (\AA , $^\circ$).

I	J	CgI...CgJ	Inter-plane angle	CgI_perp	CgI_offset
4	5 ⁱ	3.973 (2)	8.2 (2)	1.327 (2)	1.831 (2)
5	4 ⁱⁱ	3.973 (2)	8.2 (2)	3.745 (2)	1.327 (2)

Cg4 and Cg5 denote the centroids of the rings C18–C23 and C27–C32, respectively. CgI/CgJ is the distance between ring centroids. The inter-plane angle is that between the planes of the rings I and J. CgI_perp is the perpendicular distance of CgI from ring J. CgI_offset is the distance between CgI and perpendicular projection of CgJ on ring I. Symmetry codes: (i) $-x+1, y+1/2, -z+1/2$; (ii) $-x+1, y-1/2, -z+1/2$.

signals is \sim twice lower, than it is expected for the given molecular formula.

The electronic excitations nature of **1** was analyzed with ESSA method [43]. It is the generalization to the contemporary TDDFT calculational scheme of the earlier approach, which was initially elaborated for the π -electronic methods in the middle 1970s [44]. The special “electronic excitation localization indices”, L_i (%), help to elucidate the degree of participation of the functional groups and submolecular fragments of the studied molecules in formation of the electronic transitions in their UV–vis spectra. “Charge transfer indices”, I_{ij} (% of elementary electric charge), devoted to show in details the directions of the electronic density redistribution between the atoms and more complicated subunits of the molecule. These indices are much more informative in comparison with the traditional “charge changes” in Δq format, which reflect only the final result of the excited state intramolecular electron density redistribution.

The molecular plots of ESSA indices for the long-wavelength transition in the electronic absorption spectrum of **1** are shown in Table 4.

Parameters of the electronic transition: wavelength, wave-number and oscillator strength. Owing to the symmetry of **1**, redistribution of molecular indices is shown only on one of the identical parts of this molecule. Together with electronic localization indices (L_i , red), their % difference from the case of “all-atoms proportional participation” in the electronic excitation is shown as well.

Electronic absorption spectra calculation reveals partial restoration of π -conjugation in compound **1** on its going from crystalline state to fluid media: long-wavelength electronic transition calculated for the isolated title molecule in the X-ray geometry was situated at 345 nm only, this means hypsochromic shift of more than 1800 cm^{-1} in comparison with its position presented in Table 4.

Our ESS-analysis had shown difference in participation of structural subunits of **1** molecule in formation of its lowest singlet excited state. The summarized electronic localization indices for the terminal benzene rings were much lower (down to 45%), than it could be expected in case of uniform involvement of all the atoms of title molecule in the electronic excitation. The main contributions was typical to oxazole and oxadiazole moieties, which exceed the median level up to 40 and 31% correspondently, while as participation of the rest two phenylene fragments is close to the average value. Generally, the electronic excitation in the studied molecule was localized on its central part, in which the changes in molecular conformation at electronic excitation should be the most prominent.

As it was emphasized earlier, the oxadiazole cycle is more electron deficient than oxazole one, thus the electric charges redistribution was expected to be directed from the second of them toward the first. Moreover, analyzing the electron density redistribution in 2,5-diphenyl-1,3-oxazole molecule, we have found that its main direction is from phenyl radical in position 5 to phenyl-2 [45]. Both the discussed directions are coinciding

Table 4
Long-wavelength electronic transition in UV absorption spectrum of **1** (*b3lyp/cc-pvdz* and ESSA).

LW electronic transition	Localization indices, L_i	Net charge changes, Δq	Charge transfer indices, l_{ij}
369 nm 27110 cm ⁻¹ $f=0.263$			

Parameters of the electronic transition: wavelength, wavenumber and oscillator strength. Owing to the symmetry of **1**, redistribution of molecular indices is shown only on one of the identical parts of this molecule. Together with electronic localization indices (L_i , red), their % difference from the case of “all-atoms proportional participation” in the electronic excitation is shown as well.

mutually in **1** molecule. Our quantum-chemical modeling confirms these preliminary assumptions. Calculated excited state net charge changes (Δq) and charge transfer indices (l_{ij}) reveal redistribution of electron density from the periphery of **1** molecule to its center with predominant electric charge removal from the oxazole cycles toward the oxadiazole ones and its neighboring benzene rings. However, the resulted additional excited state polarization of **1** is not high: the calculated vector difference of its ground and excited states dipole moments – the quantitative measure of the excited state electric charges redistribution – was no more than 4.5 D. Thus, the expected sensitivity of **1** to solvent polarity should not be significant.

The excited state molecular geometry of **1** was modeled in *td/b3lyp/cc-pvdz* scheme and dramatic changes in the S_1 -state conformation was revealed (Fig. 3). First of all, the title molecule became asymmetric again in its structurally relaxed electronically excited state – inter-cycle planes angles demonstrate changes of different extent. The most significant decrease was detected for the angles between the planes of the central oxadiazole cycle and its neighboring phenyl moieties (from $\sim 38^\circ$ in S_0 to $\sim 21^\circ$ and $\sim 17^\circ$ in S_1). The angles between the *ortho*-disubstituted phenylenes and oxazole cycles planes were changed in opposite directions: from $\sim 30^\circ$ in S_0 to $\sim 34^\circ$ and $\sim 24^\circ$ in S_1 . Geometry of the peripheral parts of **1** remained practically the same with the terminal phenyls almost coplanar to the attached oxazole cycles. For comparison reasons, the ground and excited state geometries of **1** were superimposed in space in Fig. 3. Increased S_1 -state sterical hindrance was partially smoothed by definite space distortion of the *ortho*-phenylene moieties: the torsion angles formed by their

chemical bonds in the *ortho*-positions were increased to $\sim 22^\circ$ and $\sim 19^\circ$, while as in the ground state they were less than 10° . Thus, the molecule of compound **1** can be classified as molecular machine, which works like subnanodimensional spring, which can be compressed at absorption of light and returned to its usual shape after fluorescence emission.

Generally, one can conclude, that in the lowest singlet excited state the **1** molecule became more compact and “a bit” more conjugated. The last circumstance reflects itself in significant long-wavelength shift of the calculated S_0 – S_1 electronic transition for the excited state optimized molecular geometry, which is usually considered as a model for position of fluorescence spectrum (vertical transition of the structurally relaxed excited state to its corresponding Franck–Condon ground state), 510 nm/19620 cm⁻¹. Difference in energy between positions of the long-wavelength electronic transitions calculated for the ground- and excited state optimized molecular geometries is the theoretical estimate of the fluorescence Stokes shift in vacuo. In case of compound **1**, the predicted in such a way Stokes shift was close to 7500 cm⁻¹ and should be considered as abnormally high. It is worth to emphasize that computed $\Delta\nu_{ST}$ satisfactory reproduces the experimentally observed values taking into account also the possible contributions of intermolecular solvent–solute interactions (see Section 4.3).

The last circumstance, which needs to be clarified, is the asymmetrization of the investigated molecule in the partially flattened structurally relaxed excited state. The reason of such behavior could be intramolecular interactions only, because the quantum-chemical calculations were made for the isolated molecule in vacuo. Analyses of the S_1 -optimized molecular geometry of **1** have shown spatial approaching of its oxazole cycles: the distance between their calculated ring centroids was 3.84 Å only, this is close to the effective Van-der-Vaals thickness of an aromatic ring, ~ 3.4 Å (doubled half-thickness). The planes of the oxazole cycle are nearly parallel – the angle between them was $\sim 14^\circ$. Based on this observation, we have to assume the excited state of the structurally relaxed **1** molecule as having definite features of an “intramolecular excimer” with shortened π – π contacts between some of its (hetero) aromatic moieties. Spatial attraction between the discussed oxazole rings, probably plays the role of a factor making the excited title molecule more compact and asymmetric. Similar behavior was recently reported by us also for nitro-dimethylamino substituted *ortho*-POPOPs [25].

Finally, the excited state planarization of the title molecule requires high-amplitude intramolecular motions. This allows us to expect the existence of media viscosity regulation of the excited state structural relaxation process in this case.

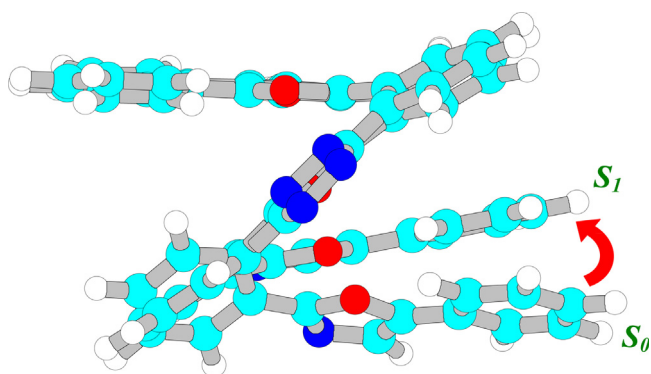


Fig. 3. Calculated ground and excited state molecular geometries of compound **1** aligned in space by one of oxazole cycles of both S_0 and S_1 -optimized structures.

Table 5

Spectral properties of 2,5-bis[2-(2-phenyl-1,3-oxazol-5-yl) phenyl]-1,3,4-oxadiazole in solvents of different nature.

Solvent	E_T^N	λ_a nm	ν_a cm ⁻¹	λ_f cm	ν_f cm ⁻¹	$\Delta\nu_{ST}$ cm ⁻¹	ϕ	τ ns	k_f s ⁻¹	k_d s ⁻¹
Hexane	0.009	308	32470	416	24040	8430	0.54	2.69	2.0×10^8	1.7×10^8
Toluene	0.099	310	32260	428	23360	8900	0.54	2.99	1.8×10^8	1.5×10^8
1,4-dioxane	0.164	311	32150	432	23150	9000	0.47	2.21	2.1×10^8	2.4×10^8
Ethyl acetate	0.228	312	32050	439	22780	9270	0.45	2.91	1.5×10^8	1.9×10^8
1,2-dichloroethane	0.327	310	32260	433	23090	9170	0.55	3.18	1.7×10^8	1.4×10^8
DMF	0.386	314	31850	447	22370	9480	0.43	2.10	2.0×10^8	2.7×10^8
Acetonitrile	0.460	312	32050	442	22620	9430	0.44	2.81	1.6×10^8	2.0×10^8
Ethanol	0.654	315	31750	449	22270	9480	0.41	2.95	1.4×10^8	2.0×10^8

λ_a , ν_a , λ_f , ν_f : positions of the long-wavelength absorption and fluorescence bands; $\Delta\nu_{ST}$: fluorescence Stokes shift; ϕ and τ : fluorescence quantum yield and mean lifetime; k_f and k_d : rate constants of primary photophysical processes: fluorescence emission and radiationless decay correspondently, calculated by traditional equations $k_f = \phi/\tau$; $k_d = (1 - \phi)/\tau$.

4.3. Absorption and steady-state fluorescence spectra

Electronic absorption and emission spectra of **1** were measured in the series of aprotic solvents of different polarity and ethyl alcohol as an example of a protic solvent. The corresponding numerical data is collected in Table 5, solvatochromic behavior of the title compound is shown in Fig. 4.

Absorbing in the near UV, quite similarly to *ortho*-POPOPs [26], compound **1** emits fluorescence in blue region having abnormally high Stokes shifts of above 8000 cm⁻¹. This is the result of its molecule' excited state structural relaxation discussed in the previous section. Both the experimental absorption and emission spectra demonstrate slight tendency to red shift with media polarity. Generally, solvent polarity makes a contribution of no more than 1000 cm⁻¹ to the total Stokes shift value. This reflects quite a low extent of electron density redistribution at electronic excitation discussed in the Section 4.2.

Fluorescence quantum yields of **1** are high enough (0.4–0.5) demonstrating intermediate efficiency of its lowest singlet excited state radiationless dissipation. The same tendency is typical to lifetimes. Primary photophysical processes rate constants (radiative, k_f , and radiationless S_1 -state deactivation, k_d) are of nearly the same order in all the solvents examined.

Data for protic ethanol does not fall out of the common tendency, this means intermolecular hydrogen bonding have insignificant effect on the excited state structural relaxation of **1** and its photophysics as well.

4.4. Time-resolved experiments

To visualize the process of the excited state structural relaxation, time-resolved fluorescence spectra were measured for compound **1** solutions in three alcohols of different viscosity: 2-propanol ($\eta = 1.77$ cP), ethylene glycol (13.6 cP) and glycerol (945 cP, 25 °C), Fig. 5.

Among these three alcohols, the observed spectral shifts are the fastest in 2-propanol, when the changes in maxima position were completed at ~ 1 ns after the IRF maxima time. The relaxation process is the slowest in glycerol, when changes in spectra last until ~ 10 ns. Ethylene glycol demonstrates intermediate behavior. All the discussed features are connected with the retarding of the excited state structural relaxation of the title molecule by the media viscosity.

The excited state structural relaxation rates were estimated with the approach used in our initial paper on *ortho*-POPOPs excited state dynamics [26]. In connection with our hypothesis (Section 4.2) that structurally relaxed excited state of **1** has definite features of intramolecular excimer and applying all the assumptions made on this purpose in [26], we again decided to treat the obtained time-resolved fluorescence data in the discrete “two-states” model rather than in alternative “continuum relaxation” model.

The initial time-resolved fluorescence spectrum (near the “zero time”) and the final one (when practically no further changes in spectral position and shape are observed) satisfactory reproduce

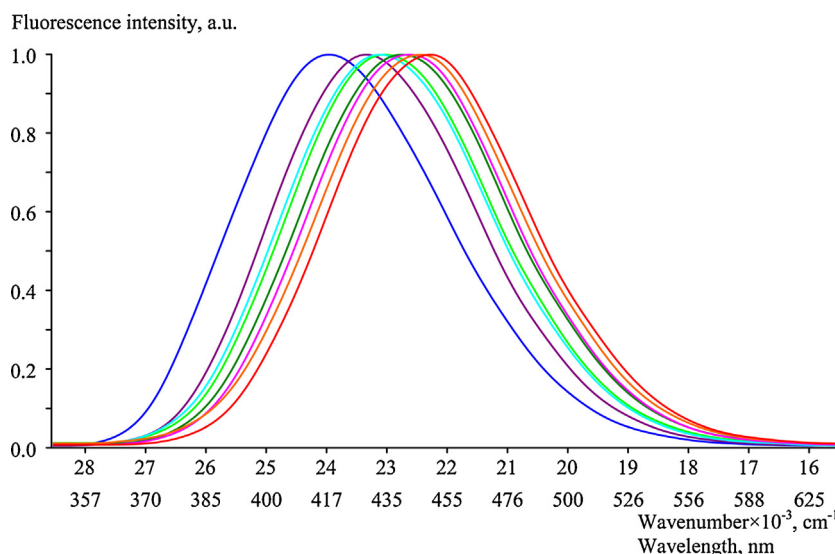


Fig. 4. Solvent effect on fluorescence spectra of compound **1** (from left to right: hexane, toluene, 1,4-dioxane, 1,2-dichloroethane, ethyl acetate, acetonitrile, DMF, ethanol).

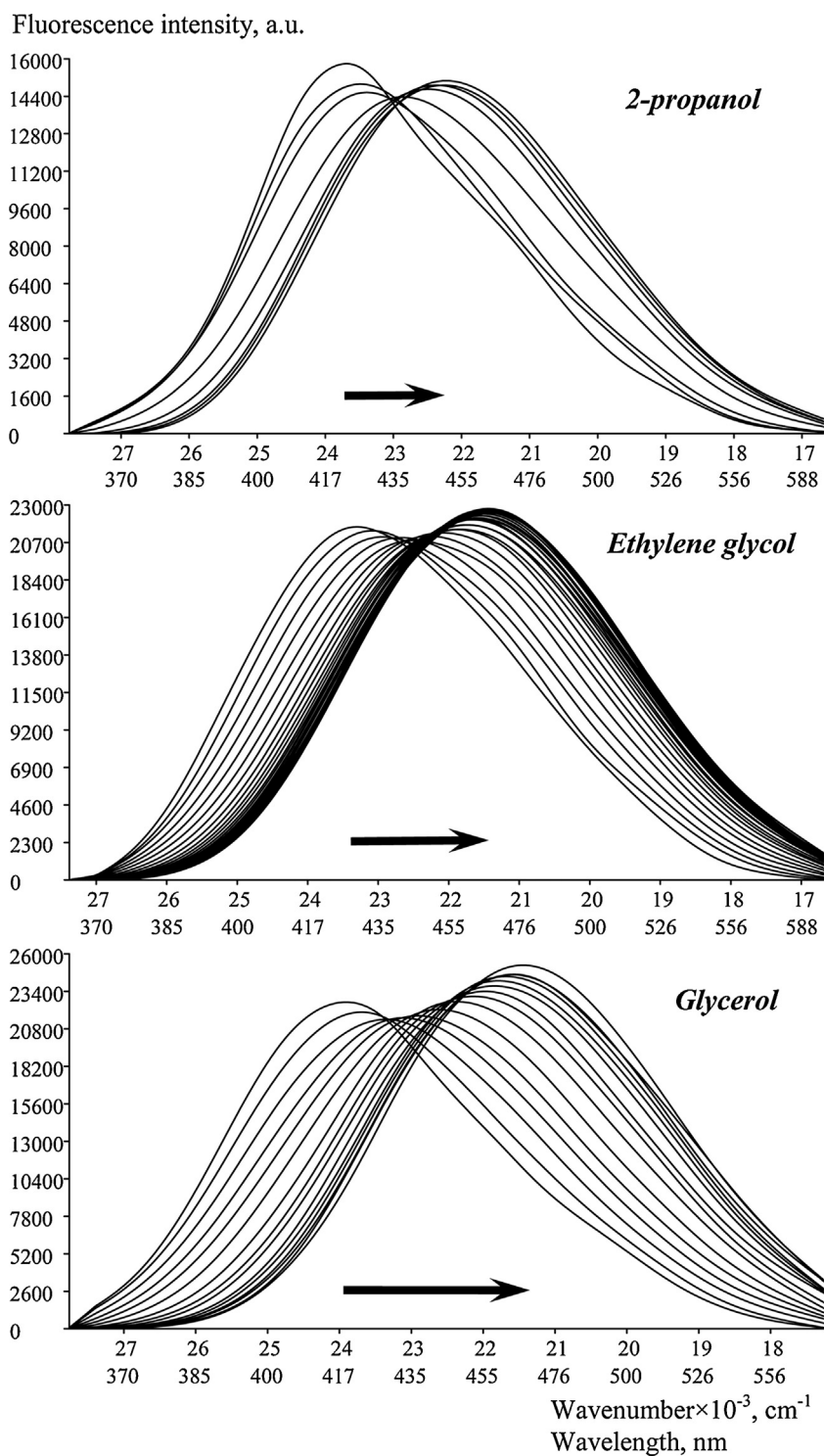


Fig. 5. Time-resolved fluorescence spectra of **1** in 2-propanol, ethylene glycol and glycerol, normalized by the area under the spectral curves. 2-propanol: $-0.2, -0.1, 0, 0.3, 0.6, 0.9, 1.9$ ns. Ethylene glycol: $-0.3, -0.2, -0.1, \dots, .23$ ns (with 0.1 ns step). Glycerol: $-0.2, 0, 0.2, 0.4, 0.6, 0.9, 1.4, 1.9, 2.4, 3.4, 4.5, 5.5, 6.5, 7.5, 9.5$ ns. "Zero time" corresponds to time moment, when the instrument response function (IRF) intensity is maximal. Arrows show the approximate spectral maxima shifts during the excited state structural relaxation of **1** in the given solvents.

the general shape of the stationary fluorescence spectrum in the given solvent (Fig. 6). This is an additional argument in favor of the discrete model.

First, the time-resolved fluorescence spectra at each time moment were deconvoluted with the spectra of all the existed excited-state interacting species (in manner, like it was shown in Fig. 6), thus we obtain for them "pure" fluorescence decay

functions, at wavelengths of maxima in the emission spectra of all the species involved. Then these decay functions were treated together to estimate the excited state chemical reactions (photo-transformations) rates and real excited state species lifetimes.

The Eq. (1) derived in [26] was applied for obtaining quantitative parameters of the excited state conversion of the species X^* into A^* (in the present case – initial and structurally

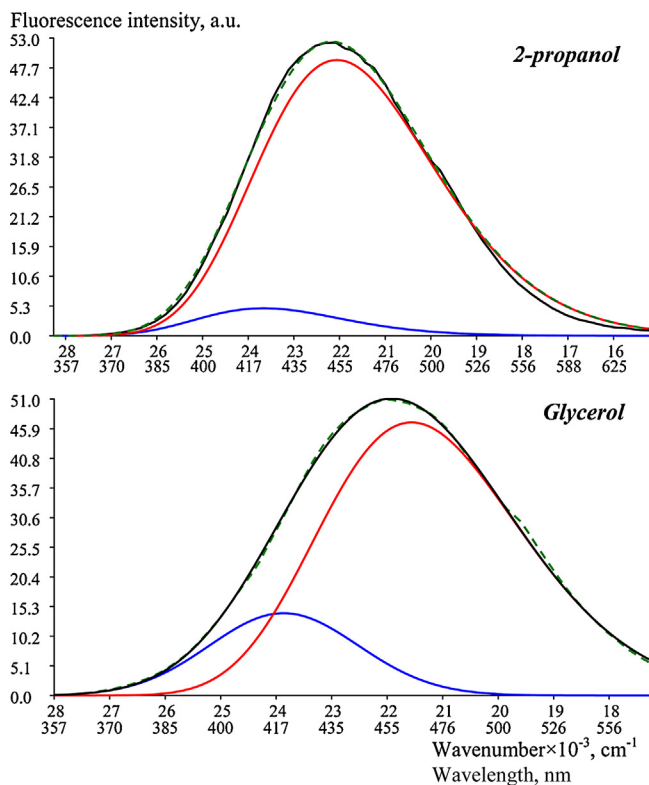


Fig. 6. Deconvolution of the stationary fluorescence spectra of **1** in 2-propanol (up) and glycerol (down) with the initial (blue line) and the final (red line) spectra derived from the time-resolved experiment (dashed green – the sum of the deconvoluted spectra). (For interpretation of the references to colour in this figure legend, the reader is referred to the web version of this article.)

relaxed states of **1**).

$$\frac{Fl_A(t_2) - Fl_A(t_1)}{\int_{t_1}^{t_2} IRF(t) dt} = b \times \frac{k_f^A}{S_A} + \sum_{X=B,C,\dots} k_{X-A} \times \frac{k_f^A \times S_X}{k_f^X \times S_A} \times \frac{\int_{t_1}^{t_2} Fl_X(t) dt}{\int_{t_1}^{t_2} IRF(t) dt} - \frac{1}{\tau_A} \times \frac{\int_{t_1}^{t_2} Fl_A(t) dt}{\int_{t_1}^{t_2} IRF(t) dt} \quad (1)$$

Here $Fl_A(t)$ and $Fl_X(t)$ – fluorescence intensities (at their spectra maxima) of A and X at time moment t , taken from the “pure” (deconvoluted) decay curves of A and X; $IRF(t)$ – instrument response function; τ_A – lifetime of A; k_f^A , k_f^X – fluorescence emission rate constants for A and X; S_A , S_X – areas under the normalized fluorescence spectra of A and X; k_{X-A} – rate constant for the excited state chemical reaction (phototransformation) of X into A. The limits of integration, times t_1 (starting point) and t_2 (all the time moments between t_1 and final time point of the measured decay curve) are selected to get maximally available amount of data points for linear least squares method (LSM) treatment. Expression in the left part of the Eq. (1) is the dependent variable,

integral ratios in the right part are independent variables, $k_{X-A} \times \frac{k_f^A \times S_X}{k_f^X \times S_A}$ and τ_A are calculated as slopes, $b \times \frac{k_f^A}{S_A}$ – as the intercept parameters of the multi-dimensional linear LSM. Very often the normalizing coefficient $\frac{k_f^A \times S_X}{k_f^X \times S_A}$, needed to estimate the k_{X-A} rate constant “true value”, is close to 1, the present case seems not an exception.

Alternatively to (1) its differential version (2) can be applied, which gives more reliable results for the starting time intervals of the decay curves and, correspondingly, for the faster phototransformations rates. First derivative of the decay curve, $\frac{\partial Fl_A(t)}{\partial t}$, is taken numerically in this case, all the decay data treated by (2) need preliminary (numerical) smoothing, for example, by simple procedures of Savitzky and Golay [46].

$$\frac{\partial Fl_A(t)}{\partial t} = b \times \frac{k_f^A}{S_A} \times IRF(t) + \sum_{X=B,C,\dots} k_{X-A} \times \frac{k_f^A \times S_X}{k_f^X \times S_A} \times Fl_X(t) - \frac{1}{\tau_A} \times Fl_A(t) \quad (2)$$

The Eqs. (1) and (2) are the good alternative to the popular during several decades approach for the estimation of the excited state phototransformations rates based on poly-exponential approximation of fluorescence decay curves with further application of the Birks et al. scheme [47]. Treatment of the time-resolved fluorescence spectra of **1** with the above mentioned approaches allowed us to estimate its excited state structural relaxation rates in the given protic solvents: $3.4 \times 10^9 \text{ s}^{-1}$ in 2-propanol, $2.7 \times 10^9 \text{ s}^{-1}$ in ethylene glycol and $1.4 \times 10^9 \text{ s}^{-1}$ in glycerol. The obtained values are rather high in comparison, for example, with **1** fluorescence emission rate constant, however, generally the discussed structural relaxation process is slower, than the examined solvents relaxation rates. Thus we can classify the obtained rate constants as characteristic of the intramolecular process, first of all. However, they reveal also definite retarding of the excited state structural relaxation rate of the title molecule by the media viscosity.

4.5. Prospects of viscosity sensing with compound 1

Owing to the general need in fluorescent viscosity probes giving tolerable results and sensing simultaneously less number of the other interfering parameters of their surrounding (solvent polarity, humidity, etc.), we decided to test our title compound for this purpose as well.

The toluene–polystyrene mixtures were chosen as the inert and suitable model surrounding with its viscosity regulated by the amount of the polymer in the mixed solution. Polarity of such solutions should be nearly the same as that for the pure toluene, thus all the observed spectral effects will be caused by the variation of the media viscosity.

The kinematic viscosity for solutions of **1** in toluene containing different concentrations of polystyrene was measured directly with glass flow viscosimeter of BPZh-4 type at 25 °C before taking their fluorescence spectra (Table 6) and then recalculated into

Table 6
Preparation of toluene–polystyrene solutions with varied viscosity.

Solution	Polystyrene mass, g	Toluene volume, ml	Mean flow time through the capillar, s	Kinematic viscosity, mm ² /s	Density of poly-styrene/toluene solution, g/cm ³	Dynamic viscosity, cP	Fluorescence spectrum of 1 center of mass, cm ⁻¹
0	0	10	25	0.76	0.862	0.66	23030
1	0.1	10	41	1.24	0.863	1.07	23050
2	0.2	10	72	2.18	0.866	1.89	23240
3	0.3	10	103	3.13	0.868	2.72	23390
4	0.4	10	150	4.55	0.871	3.96	23550
5	0.5	10	208	6.31	0.872	5.50	23840
6	0.6	10	273	8.28	0.874	7.24	24060

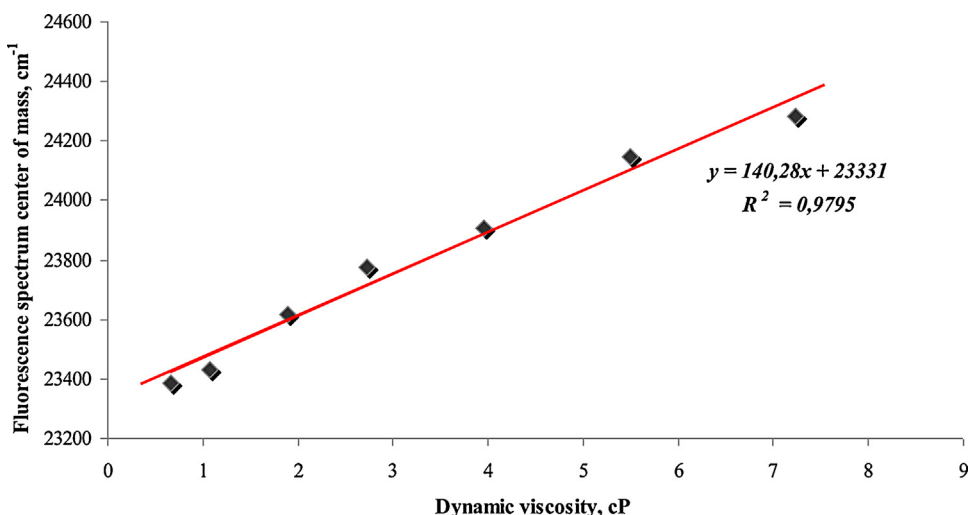


Fig. 7. Toluene–polystyrene system fluorescent dynamic viscosity sensing with compound 1.

dynamic viscosity by introducing the polystyrene-toluene solutions density data.

The emission spectrum of **1** is rather broad, thus to obtain more adequate estimate of its position, we calculated the center of mass (with the purpose to decrease the experimental errors). Fig. 7 demonstrates the linear spectral shift toward the shorter wavelengths with the increase of viscosity and principle suitability of **1** to color-change fluorescent viscosity sensing. Covering the low viscosity interval only (below 8 cp) was reasoned by the parameters of the chosen flow viscosimeter. Enlargement of the dynamical interval of viscosity sensing with the title compound and an attempt to discriminate polarity and viscosity effects will be the subject of our future experiments.

5. Conclusions

New sterically hindered representative of the *ortho*-POPOP family with the semi-helix-like molecular shape, 2,5-bis[2-(2-phenyl-1,3-oxazol-5-yl) phenyl]-1,3,4-oxadiazole, **1**, was synthesized.

X-ray structural analysis and quantum-chemical modeling reveal significant asymmetrization and decrease of **1** molecular volume in the crystalline state compared to that in fluid media. The intermolecular π - π contacts in the crystalline lattice and weak intermolecular hydrogen bonds of C–H $\cdots\pi$ type are shown as the reasons for such behavior.

Intramolecular sterical hindrance and resulted non-planar structure violates π -conjugation between (hetero) aromatic rings of **1** in the ground state, this causes significantly blue shifted absorption spectra of the title molecule. Contrary to the ground state, compound **1** undergoes substantial planarization in the electronically excited state resulted in partial restoration of intramolecular π -conjugation, which was revealed both theoretically and experimentally with the calculated and observed abnormally high fluorescence Stokes shifts.

The title compound demonstrates slight positive solvatofluorochromism owing to the specific excited state redistribution of electron density and negative solvatofluorochromism in highly viscose media.

The excited state structural relaxation typical to **1** could be considered as an example of large-amplitude intramolecular motions, thus it is regulated by the media viscosity: the excited state relaxation rate retarding in solvents of increased viscosity,

2-propanol, ethylene glycol and glycerol, was revealed with the time-resolved fluorescence spectroscopy data.

To distinguish between the influence of solvent polarity and viscosity contributions, the title compound was tested in the mixed toluene–polystyrene system. The obtained results allow us to recommend **1** as color-changing fluorescent viscosity sensing compound.

Acknowledgement

The Authors express their gratitude to prof. J. Błażejowski (Gdansk University, Poland) for the opportunity to make the reported X-ray structural analysis of compound **1**.

Appendix A. Supplementary data

Supplementary data associated with this article can be found, in the online version, at <http://dx.doi.org/10.1016/j.jphotochem.2014.10.018>.

References

- [1] A. Credi, L. Prodi, Inner filter effects and other traps in quantitative spectrofluorimetric measurements: origins and methods of correction, *J. Mol. Struct.* 1077 (2014) 30–39.
- [2] A.O. Doroshenko, Physical and chemical principles for creation of highly effective organic luminophores with abnormally high Stokes shift, *Theor. Exper. Chem.* 38 (2002) 133–152.
- [3] V.M. Feygelman, J.K. Walker, A.R. Katrizky, Z. Deda-Szafran, Studies of sterically hindered oxadiazoles as potential fluorescent dopants for polymeric scintillators, *Chem. Scr.* 29 (1989) 241–243.
- [4] C.-W. Ko, Y.-T. Tao, J.T. Lin, K.R.J. Thomas, Light-emitting diodes based on a carbazole-derivatized dopant: origin of dopant excitation as a function of the device structure, *Chem. Mater.* 14 (2002) 357–361.
- [5] Y. Ooyama, S. Yoshikawa, S. Watanabe, K. Yoshida, Molecular design of novel non-planar heteropolycyclic fluorophores with bulky substituents: convenient synthesis and solid-state fluorescence characterization, *Org. Biomol. Chem.* 4 (2006) 3406–3409.
- [6] B. Valuer, I. Leray, Design principles of fluorescent molecular sensors for cation recognition, *Coord. Chem. Rev.* 205 (2000) 3–40.
- [7] Y. Chen, J. Zhao, H. Guo, L. Xie, Geometry relaxation-induced large Stokes shift in red-emitting borondipyrromethenes (BODIPY) and applications in fluorescent thiol probes, *J. Org. Chem.* 77 (2012) 2192–2206.
- [8] S. Atilgan, T. Ozdemir, E.U. Akkaya, Selective Hg(II) sensing with improved Stokes shift by coupling the internal charge transfer process to excitation energy transfer, *Org. Lett.* 12 (2010) 4792–4795.
- [9] F. Vollmer, W. Rettig, E. Bircner, Photochemical mechanisms producing large fluorescence Stokes shifts, *J. Fluor.* 4 (1994) 65–69.
- [10] H. Beens, A. Weller, Excited molecular π -complexes in solution, *Org. Mol. Photophys.* 2 (1975) 159–215.

- [11] M.G. Kuzmin, L.N. Guseva, Donor-acceptor complexes of singlet excited states of aromatic hydrocarbons with aliphatic amines, *Chem. Phys. Lett.* 3 (1969) 71–72.
- [12] P. Sett, S. Chattopadhyay, P.K. Mallick, Excited state configuration of biphenyl, *Chem. Phys. Lett.* 331 (2000) 215–223.
- [13] J. He, J.L. Crase, S.H. Wadumethrige, K. Thakur, L. Dai, S. Zou, R. Rathore, C.S. Hartley, *Ortho*-phenylenes: unusual conjugated oligomers with a surprisingly long effective conjugation length, *J. Am. Chem. Soc.* 132 (2010) 13848–13857.
- [14] Z.R. Grabowski, K. Rotkiewicz, W. Rettig, Structural changes accompanying intramolecular electron transfer: focus on twisted intramolecular charge-transfer states and structures, *Chem. Rev.* 103 (2003) 3899–4031.
- [15] L.G. Arnaut, S.J. Formosinho, Excited state proton transfer reactions. I. Fundamentals and intramolecular reactions, *J. Photochem. Photobiol. A: Chem.* 75 (1993) 1–20.
- [16] S.J. Formosinho, L.G. Arnaut, Excited state proton transfer reactions. II. Intramolecular reactions, *J. Photochem. Photobiol. A: Chem.* 75 (1993) 21–48.
- [17] N.I. Nijegorodov, W.S. Downey, The influence of planarity and rigidity on the absorption and fluorescence parameters and intersystem crossing rate constant in aromatic molecules, *J. Phys. Chem.* 98 (1994) 5639–5643.
- [18] A.O. Doroshenko, Spin-orbit interaction and structural relaxation of the 1,2-bis-(5-phenyloxazolyl)-2-benzene molecule in the excited state, *Russ. J. Phys. Chem.* 74 (2000) 773–777.
- [19] C.S. Hartley, Excited-state behavior of *ortho*-phenylenes, *J. Org. Chem.* 76 (2011) 9188–9191.
- [20] T. Sato, K. Hori, M. Fujitsuka, A. Watanabe, O. Ito, K. Tanaka, Photophysical properties of bis(2,2'-bitiophen-5-yl) benzenes, *J. Chem. Soc. Faraday Trans. 94* (1998) 2355–2360.
- [21] A.O. Doroshenko, L.D. Patsenker, V.N. Baumer, L.V. Chepeleva, A.V. Van'kevich, A.V. Kirichenko, S.N. Yarmolenko, V.M. Scherschukov, V.G. Mitina, O.A. Ponomaryov, Structure of sterically hindered aryl derivatives of five-membered nitrogen containing heterocycles – *ortho*-analogs of POPOP, *Mol. Eng.* 3 (1994) 343–352.
- [22] R. Yu Iliashenko, N. Yu Gorobets, A.O. Doroshenko, New and efficient high Stokes shift fluorescent compounds: unsymmetrically substituted 1,2-bis-(5-phenyloxazol-2-yl) benzenes via microwave-assisted nucleophilic substitution of fluorine, *Tet. Lett.* 52 (2011) 5086–5089.
- [23] A.O. Doroshenko, V.N. Baumer, A.A. Verezubova, L.M. Ptyagina, Molecular structure of unsubstituted oxadiazolic analog of *ortho*-POPOP and peculiarities of conformational structure of this class of sterically hindered organic compounds, *J. Mol. Struct.* 609 (2002) 29–37.
- [24] A.O. Doroshenko, A.V. Kyrychenko, J. Waluk, Low temperature spectra of the *ortho*-POPOP molecule: additional arguments of its flattening in the excited state, *J. Fluor. 10* (2000) 41–48.
- [25] R.Y. Iliashenko, O.S. Zozulia, A.O. Doroshenko, High Stokes shift long-wavelength energy gap regulated fluorescence in the series of nitro/dimethylamino-substituted *ortho*-analogs of POPOP, *Cent. Eur. J. Chem.* 9 (2011) 962–971.
- [26] A.O. Doroshenko, A.V. Kirichenko, V.G. Mitina, O.A. Ponomaryov, Spectral properties and dynamics of the excited state structural relaxation of the *ortho* analogues of POPOP – effective abnormally large Stokes shift luminophores, *J. Photochem. Photobiol. A: Chem.* 94 (1996) 15–26.
- [27] A.O. Doroshenko, A.V. Kyrychenko, V.N. Baumer, A.A. Verezubova, L.M. Ptyagina, Molecular structure, fluorescent properties and dynamics of excited state structural relaxation of the oxadiazolic *ortho*-analog of POPOP with the additional sterical hindrance, *J. Mol. Struct.* 524 (2000) 289–296.
- [28] A.O. Doroshenko, The effect of solvent on the spectral properties and dynamics of structural relaxation of two excited-state *ortho*-analogs of POPOP with essentially different properties, *Chem. Phys. Rep.* 18 (1999) 873–880.
- [29] M.A. Haidekker, E.A. Theodorakis, Molecular rotors—fluorescent biosensors for viscosity and flow, *Org. Biomol. Chem.* 5 (2007) 1669–1678.
- [30] M.K. Kuimova, G. Yahioglu, J.A. Levitt, K. Suhling, Molecular rotor measures viscosity of live cells via fluorescence lifetime imaging, *J. Am. Chem. Soc.* 130 (2008) 6672–6673.
- [31] M.K. Kuimova, Mapping viscosity in cells using molecular rotors, *Phys. Chem. Chem. Phys.* 14 (2012) 12671–12686.
- [32] <http://ursabioscience.com/technology/viscosity-probes>.
- [33] S. Parsons, H. Flack, Precise absolute-structure determination in light-atom crystals, *Acta Cryst. A60* (2004) s61.
- [34] G.M. Sheldrick, A short history of SHELX, *Acta Cryst. A 64* (2008) 112–122.
- [35] L.J. Farrugia, ORTEP-3 for Windows – a version of ORTEP-III with a graphical user interface (GUI), *J. Appl. Cryst.* 30 (1997) 565.
- [36] A.L. Spek, Structure validation in chemical crystallography, *Acta Cryst. D65* (2009) 148–155.
- [37] W.H. Melhuish, Absolute spectrofluorometry, *J. Res. Nat. Bur. Stand. USA 76A* (1972) 547–560.
- [38] C. Reichardt, Solvatochromic dyes as solvent polarity indicators, *Chem. Rev.* 94 (1994) 2319–2358.
- [39] A.D. Becke, Density-functional thermochemistry. III. The role of exact exchange, *J. Chem. Phys.* 98 (1993) 5648–5652.
- [40] D.E. Woon, T.H. Dunning, Gaussian basis sets for use in correlated molecular calculations. III. The atoms aluminum through argon, *J. Chem. Phys.* 98 (1993) 1358–1371.
- [41] M.J. Frisch, G.W. Trucks, H.B. Schlegel, G.E. Scuseria, M.A. Robb, J.R. Cheeseman, G. Scalmani, V. Barone, B. Mennucci, G.A. Petersson, H. Nakatsuji, M. Caricato, X. Li, H.P. Hratchian, A.F. Izmaylov, J. Bloino, G. Zheng, J.L. Sonnenberg, M. Hada, M. Ehara, K. Toyota, R. Fukuda, J. Hasegawa, M. Ishida, T. Nakajima, Y. Honda, O. Kitao, H. Nakai, T. Vreven, J.A. Montgomery Jr., J.E. Peralta, F. Ogliaro, M. Bearpark, J.J. Heyd, E. Brothers, K.N. Kudin, V.N. Staroverov, T. Keith, R. Kobayashi, J. Normand, K. Raghavachari, A. Rendell, J.C. Burant, S.S. Iyengar, J. Tomasi, M. Cossi, N. Rega, J.M. Millam, M. Klene, J.E. Knox, J.B. Cross, V. Bakken, C. Adamo, J. Jaramillo, R. Gomperts, R.E. Stratmann, O. Yazyev, A.J. Austin, R. Cammi, C. Pomelli, J.W. Ochterski, R.L. Martin, K. Morokuma, V.G. Zakrzewski, G.A. Voth, P. Salvador, J.J. Dannenberg, S. Dapprich, A.D. Daniels, O. Farkas, J.B. Foresman, J.V. Ortiz, J. Cioslowski, D.J. Fox, Gaussian 09, Revision B.01, Gaussian, Inc., Wallingford, CT, 2010.
- [42] E.J. Bylaska, W.A. de Jong, N. Govind, K. Kowalski, T.P. Straatsma, M. Valiev, D. Wang, E. Apra, T.L. Windus, J. Hammond, P. Nichols, S. Hirata, M.T. Hackler, Y. Zhao, P.-D. Fan, R.J. Harrison, M. Dupuis, D.M.A. Smith, J. Nieplocha, V. Tipparaju, M. Krishnan, Q. Wu, T. Van Voorhis, A.A. Auer, M. Nooijen, E. Brown, G. Cisneros, G.I. Fann, H. Fruchtl, J. Garza, K. Hirao, R. Kendall, J.A. Nichols, K. Tsemekhman, K. Wolinski, J. Anchell, D. Bernholdt, P. Borowski, T. Clark, D. Clerc, H. Dachsel, M. Deegan, K. Dyall, D. Elwood, E. Glendening, M. Gutowski, A. Hess, J. Jaffe, B. Johnson, J. Ju, R. Kobayashi, R. Kutteh, Z. Lin, R. Littlefield, X. Long, B. Meng, T. Nakajima, S. Niu, L. Pollack, M. Rosing, G. Sandrone, M. Stave, H. Taylor, G. Thomas, J. van Lenthe, A. Wong, Z. Zhang, N.W. Chem, A Computational Chemistry Package for Parallel Computers, Version 5.1, 99, Pacific Northwest National Laboratory, Richland, Washington, USA, 2007, pp. 352–999.
- [43] A.V. Luzanov, O.A. Zhikol, Electron invariants and excited state structural analysis for electronic transitions within CIS, RPA, and TDDFT models, *Int. J. Quant. Chem.* 110 (2010) 902–924.
- [44] A.V. Luzanov, The structure of the electronic excitation of molecules in quantum-chemical models, *Russ. Chem. Rev.* 49 (1980) 1033–1048.
- [45] R.Y. Ilyashenko, E.S. Roshchina, A.O. Doroshenko, Vinilogs of 2,5-diaryloxazole with the increased intramolecular donor-acceptor interaction, *Kharkov Natl. Univ. Bull., Chem. Series 932* (2010) 9–25 (in Russian).
- [46] A. Savitzky, M.J.E. Golay, Smoothing and differentiation of data by simplified least squares procedures, *Anal. Chem.* 36 (1964) 1627–1639.
- [47] J.B. Birks, D.J. Dyson, I.H. Munro, 'Excimer' fluorescence. II. Lifetime studies of pyrene solutions, *Proc. Roy. Soc.* 75 (1963) 575–588.